

Seed-Mediated Synthesis of Colloidal 2D Halide Perovskite Nanoplatelets

Cetin Meric Guvenc^[a] and Sinan Balci^{*[b]}

Abstract: Colloidal synthesis of two-dimensional lead halide perovskite nanoplatelets (2D LHP NPLs) with a general formula of $L_2[APbX_3]_{n-1}PbX_4$ has been widely performed by using hot-injection or ligand assisted reprecipitation methods. Herein, for the first time, we report on seed-mediated synthesis of two and three monolayers ($n=2, 3$) lead halide perovskite nanoplatelets without using A-site cation halide salt (AX; A = Cesium, methylammonium, formamidinium and, X = Cl, Br, I) and long chain alkylammonium halide salts (LX; L = oleylammonium, octylammonium, butylammonium and,

X = Cl, Br, I). The nanocrystal seeds have been prepared by reacting lead (II) halide salt and coordinating ligands in a nonpolar solvent and then they have been reacted with cesium oleate, formamidinium oleate or methylamine. Our facile synthesis route enabling further understanding of the growth dynamics of LHP NPLs provides highly stable, monodisperse NPLs with very narrow absorption and emission linewidths (min. 68 meV), and high PLQY (max. 37.6%).

1. Introduction


Lead halide perovskite nanoplatelets have attracted considerable attention in recent years owing to their unique optical and optoelectronic properties. Especially, narrow absorption and emission line widths, tunable bandgaps, high exciton binding energies, high defect tolerance, and highly localized energy levels of lead halide perovskite nanoplatelets make them a great candidate for the state of the art electronic, optoelectronic, and photonic technologies.^[1–7] Optical and structural properties of the layered organic-inorganic halide perovskite nanocrystals have been extensively studied.^[8–12] Absorption and photoluminescence features give specific information about the thickness of the material, which is similar to the case of metal dichalcogenides (MoS₂, WSe₂, etc.).^[13–15] In fact, $L_2[APbI_3]_{n-1}PbI_4$ crystals for $n=1, 2, 3$ have absorption peak maxima at around 510 nm, 560 nm, and 600 nm, respectively. Also, bromide counterparts of the layered Ruddlesden-Popper perovskite phases ($L_2[APbBr_3]_{n-1}PbBr_4$) for $n=1, 2, 3$ have absorption peak maxima at around 400 nm, 430 nm, and 450 nm, respectively.^[8,11,16–17] A slight variation in the absorption and photoluminescence peak positions can be observed with the A-site cation.^[1,18] Conventionally, colloidal two-dimensional lead halide perovskite nanoplatelets (2D LHP NPLs) have been synthesized by using hot-injection or ligand assisted reprecipitation (LARP) methods.^[1,4,18–29] Specifically, in the hot-injection method, coordinating ligands and PbX_2 salts are dissolved in a

high boiling point non-polar solvent at elevated temperature and then A-site cation precursor is injected into the reaction medium.^[30] In the LARP method, LX (L = oleylammonium, octylammonium, butylammonium and, X = Cl, Br, I), lead halide (PbX_2), and AX (A = Cesium, methylammonium, formamidinium and, X = Cl, Br, I) salts are all dissolved in a polar solvent such as dimethylformamide or dimethyl sulfoxide and subsequently, proper amounts of these solutions are directly injected into nonsolvents such as toluene or hexane.^[4,18,31–33] Apart from these conventional methods, seed-mediated synthesis of strongly quantum confined MAPbI₃ nanocrystals was demonstrated.^[34] The synthesis approach requires synthesis of lead oleate and preparation of halide precursor by dissolving tetrabutylammonium iodide in oleylamine and 1-octadecene mixture at relatively high temperatures. In another recent study, Huang et al. have demonstrated synthesis of $L_2[APbX_3]_2PbX_4$ ($n=3$) LHP NPLs and nanocubes in a nonpolar solvent by carrying out spontaneous crystallization.^[19] However, they were not able to monitor optical properties of the synthesized nanocrystal seeds and growing steps of the nanocrystals due to extremely fast reaction rate.^[19] Recently, Mehetor et al. combined $PbBr_2$, oleic acid, and oleylamine at elevated temperatures, and then cooled the reaction mixture down to room temperature. Subsequently, the prepared reaction mixture was reacted with Cs-oleate at room temperature and nanoplatelets were generated.^[35–36] In another study, Udayabhaskararao et al. proposed that Pb^0 metallic seeds were formed in the early stage of the hot injection method and, consequently, the Pb^0 seeds provided nucleation sites for the perovskite layers.^[37] Nevertheless, up until now, synthesis of LHP NPLs from nanocrystal seeds has not been demonstrated.

Herein, for the first time, we show seed-mediated synthesis of very thin LHP NPLs by using widely used ligands and precursors in a hot injection method. The uniqueness of this method allows us to synthesize monodisperse $L_2[APbX_3]_2PbX_4$ NPLs, $n=2, 3$, without using LX or AX salts and polar solvents.

[a] C. M. Guvenc
Department of Materials Science and Engineering
Izmir Institute of Technology, 35430 Izmir (Turkey)

[b] Assoc. Prof. Dr. S. Balci
Department of Photonics
Izmir Institute of Technology, 35430 Izmir (Turkey)
E-mail: sinanbalci@iyte.edu.tr

 Supporting information for this article is available on the WWW under <https://doi.org/10.1002/cnma.202100315>

Importantly, our facile synthesis route provides highly stable, monodisperse NPLs with very narrow absorption, photoluminescence line widths, and high PLQY. Additionally, the synthesized nanocrystal seeds can be directly used in halide exchange reactions by preserving the thickness of the nanoplatelets. The nanocrystal seed enabled halide exchange reaction indeed provides facile tuning of optical properties of 2D LHP NPLs. Finally, we monitored the seed mediated growth of 2D NPLs by using ultraviolet-visible absorption spectroscopy.

2. Results and discussion

Figure 1 shows schematic representation of the seed mediated synthesis of $L_2[MAPbX_3]_{n-1}PbX_4$ NPLs for $n=2, 3$. Diluted MA solution (33 wt% in ethanol) in hexane was used for A-site cation precursor. Note that, in the ionic metathesis reaction, the proton required for the formation of $CH_3NH_3^+$ comes from the oleic acid.^[38–39] Similarly, in the seed-mediated synthesis, MA was protonated by the available oleic acid molecules in the nanocrystal seed colloid. The same synthesis route was applied for the synthesis of $L_2[CspbX_3]_{n-1}PbX_4$, and $L_2[FAPbX_3]_{n-1}PbX_4$ NPLs. Indeed, Cs-oleate and FA-oleate were used as A-site cation precursor for the synthesis of $L_2[CspbX_3]_{n-1}PbX_4$, and $L_2[FAPbX_3]_{n-1}PbX_4$ NPLs. Therefore, as shown in Figure 1, the seed colloid was mixed with A-site cation precursors and then the solution was injected into hexane for the synthesis of NPLs.

Figure 2a shows absorption spectra of $PbBr_2$, and PbI_2 nanocrystal seeds, and the TEM images of the nanocrystal seeds were shown in Figure 2b and c, respectively. The synthesized nanocrystal seeds are nearly in circular shape and their diameters are around 2–3 nm. Furthermore, the PbI_2 nanocrystals scatter incident red laser light (Figure S1), and hence

observation of Tyndall effect suggests the existence of the nanocrystal colloid. It should be also noted that the synthesized PbI_2 nanocrystal seeds demonstrated in this work show similar optical and morphological characteristics with a study previously demonstrated by Hassan et al.^[34] On the other hand, the synthesized $PbBr_2$ nanocrystal seeds are mixture of $PbBr_2$ nanocrystals and L_2PbBr_4 NPLs. Adding some amount of oleylammonium bromide salt provides direct transformation of $PbBr_2$ nanocrystals to L_2PbBr_4 NPLs (see Figure S2a). It should be also noted that formation of some amount of L_2PbBr_4 NPLs in $PbBr_2$ nanocrystal seed colloid indicates that synthesized oleylammonium bromide amount may be enough to produce some L_2PbBr_4 NPLs. However, in the iodide containing NPLs, we did not observe any L_2PbI_4 formation without adding extra alkylammonium iodide salt (see Figure S2b). This may explain higher stability and PLQY of $L_2[APbBr_3]_{n-1}PbBr_4$ than $L_2[APbI_3]_{n-1}PbI_4$ NPLs. In Figure 2a, the absorption peak at around 300 nm clearly demonstrates the existence of the $PbBr_2$ nanocrystal seeds. In a previous study, Grisorio et al. observed a similar broad band absorption at around 300 nm, which is mainly caused by $PbBr_2$ and $PbBr_3^-$ bromoplumbate species.^[40] Note that bulk $PbBr_2$ crystals have an excitonic absorption peak at around 326 nm.^[41] Further, L_2PbBr_4 NPLs have an excitonic absorption peak at around 397 nm, which is nearly the same absorption peak position to the previously demonstrated colloidal L_2PbBr_4 NPLs by Weidman et al.^[18] The PbI_2 crystals, being a layered structure, consist of strongly bonded I–Pb–I layers where weak van der Waals forces are present in the interlayers.^[42] Indeed, intercalation of A-site cations to the layered PbI_2 structures produces perovskite structure.^[43] In the seed mediated synthesis of $L_2[APbX_3]_{n-1}PbX_4$ NPLs, the PbX_2 nanocrystals were used as seeds. Therefore, adding A-site cations to the seed solution produces $L_2[APbX_3]_{n-1}PbX_4$ type 2D

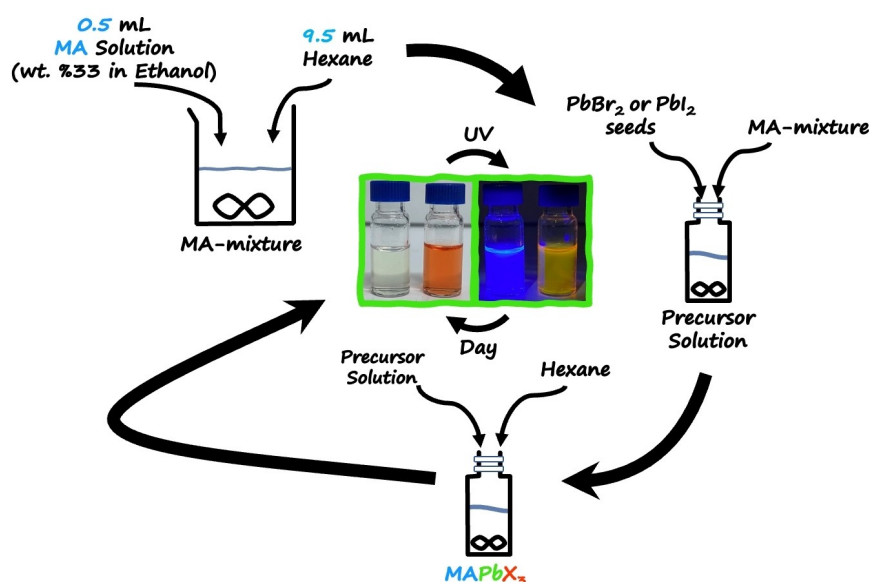


Figure 1. Seed mediated synthesis of $L_2[MAPbX_3]_{n-1}PbX_4$ NPLs. Proper amount of MA precursor was mixed with seed nanocrystals. The precursor solution was injected into hexane for the synthesis of $L_2[MAPbX_3]_{n-1}PbX_4$ NPLs. The synthesis route was also applied for all A-site cations (Cs, MA, and FA) used in this work. Cs-oleate and FA-oleate were used as A-site cation precursors for the synthesis of $CspbX_3$, and $FAPbX_3$ NPLs, respectively.

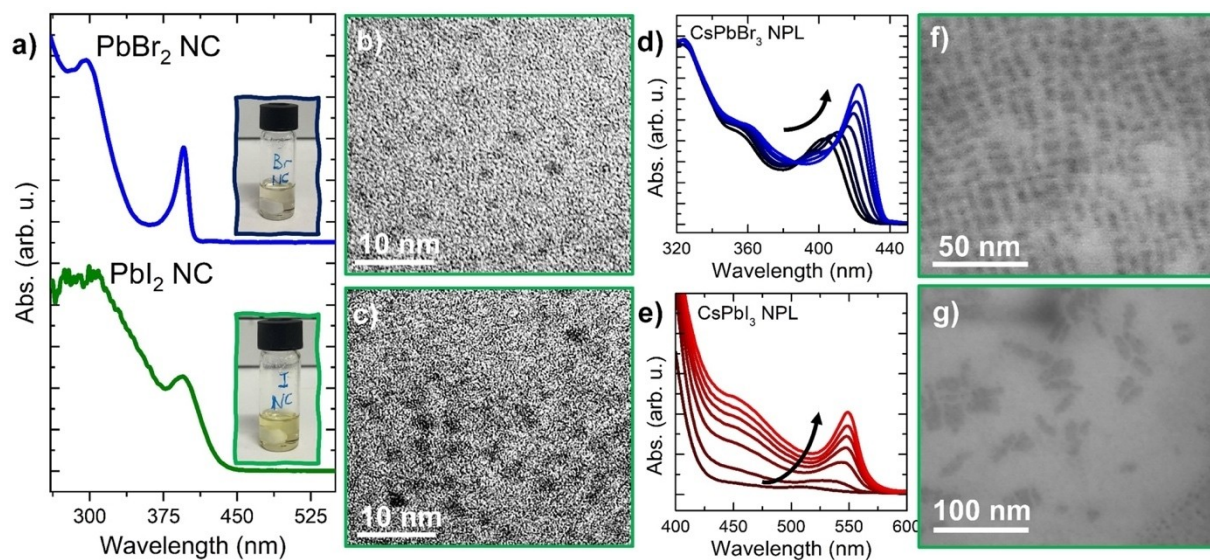


Figure 2. Seed mediated synthesis of $L_2[CsPbBr_3]PbBr_4$ and $L_2[CsPbI_3]PbI_4$ NPLs ($n=2$). (a) Absorption spectra of $PbBr_2$ and PbI_2 nanocrystal seeds. (b,c) TEM images of $PbBr_2$ and PbI_2 nanocrystals, respectively. In-situ absorption spectra of (d) $L_2[CsPbBr_3]PbBr_4$, and (e) $L_2[CsPbI_3]PbI_4$ NPLs in hexane during the seed-mediated synthesis of NPLs; each spectrum is taken after ~ 1 min. STEM images of (f) $L_2[CsPbBr_3]PbBr_4$, and (g) $L_2[CsPbI_3]PbI_4$ NPLs.

perovskite structure, and therefore, we obtain NPLs with $n=2, 3$ in the seed mediated synthesis. The growth of $L_2[CsPbBr_3]PbBr_4$ and $L_2[CsPbI_3]PbI_4$ NPLs were followed by in situ ultra-violet-visible absorption measurements. Figure 2d and e shows alteration of absorption spectra of the colloid during the growth of the nanoplates. In the first stage, small intermediate nanocrystals having a broad excitonic absorption peak are formed. During nanocrystal growth, the excitonic absorption peak shifts to longer wavelengths, and, concurrently, the linewidth of the excitonic absorption peak is narrowed. In the final stage of the growth, $L_2[CsPbBr_3]PbBr_4$ and $L_2[CsPbI_3]PbI_4$ NPLs are formed and excitonic sharp absorption peaks are observed at 429 and 556 nm, respectively. Additionally, powder XRD patterns of $L_2[APbX_3]PbX_4$ samples were shown in Figure S3. Periodic peaks in the XRD pattern indicate 4.3 nm stacking distance between NPL superstructure.^[18,35,44] The STEM images in Figure 2f and g reveal that the nanoparticles are of platelet morphology. In fact, a close inspection of the STEM images indicates that the $L_2[CsPbBr_3]PbBr_4$ NPLs have very small lateral dimensions, which are very close to $10\text{ nm} \times 3\text{ nm}$. On the other hand, the $L_2[CsPbI_3]PbI_4$ NPLs have at least two times larger lateral dimension than the $CsPbBr_3$ NPLs, owing to the fact that the weak chemical bonds between Pb–I atoms are more easily broken and reformed than the chemical bonds between Pb–Br atoms.^[45] It should be emphasized here that the synthesized NPLs in this work have smaller lateral dimension than the previously reported nanoplatelets because of the growth of NPLs from individual nanocrystal seeds.^[18,31]

We now turn our attention to understand the effects of the ligand molar ratio and Cs-oleate amount on the optical and chemical properties of LHP NPLs. In order to reach this goal, nanocrystal seeds with varying ligand molar ratios (OLAM/OA = 2:1, 2:1.5, 2:2) were prepared and subsequently, the nanocrystal seeds were reacted with a fixed volume of Cs-oleate as

shown in Figure 3a. The absorption spectra of the initial stage of the synthesis were shown as dashed lines in Figure 3a. In the initial stage, all of the synthesized LHP nanocrystals having various ligand molar ratios, have a single broad absorption peak, which may indicate formation of very small intermediate particles. As it is well known, the thickness of NPLs can be precisely controlled, which provides a very sharp absorption and PL spectra due to the quantum confined nature of NPLs in one dimension.^[1,4,18,20] When the reaction was complete, the absorption peaks (continuous lines in Figure 3a) of the samples were indeed slightly red shifted. It should be noted here that only 2:1 nanocrystal seeds have a single sharp peak at around 550 nm, which clearly indicates the formation of $L_2[CsPbI_3]PbI_4$ ($n=2$) NPLs. Synthesized NPLs from 2:1.5 and 2:2 nanocrystal seeds are combination of $L_2[CsPbI_3]_{n-1}PbI_4$ NPLs with $n=2, 3$. Moreover, in NPLs and magic size clusters (MSCs), the crystal growth occurs by addition of another monolayer on the nanocrystals. In fact, the growth of the NPLs and MSCs can be realized by observing discrete jumps to higher wavelengths in the absorption spectrum. Conversely, in the growth of quantum dots, continuous red shift in the absorption spectrum of the quantum dots has been observed.^[46] Therefore, the observed second absorption peak at around 575 nm implies growth of $n=3$ NPLs. On the other hand, similar experiments were performed by increasing the Cs-oleate volume from $5\ \mu\text{l}$ to $10\ \mu\text{l}$ and then $15\ \mu\text{l}$ in the reactions for all of the ligand molar ratios as shown in Figure 3b and c. At the beginning of the reaction, as shown in Figure 3b, we observe single absorption and PL peaks, which are slightly red shifted by decreasing the ligand molar ratios and increasing Cs-oleate amount. Therefore, the red shift observed in the absorption spectra implies that increasing OA amount causes formation of slightly larger intermediate nanocrystals. In the final stage, the measurements

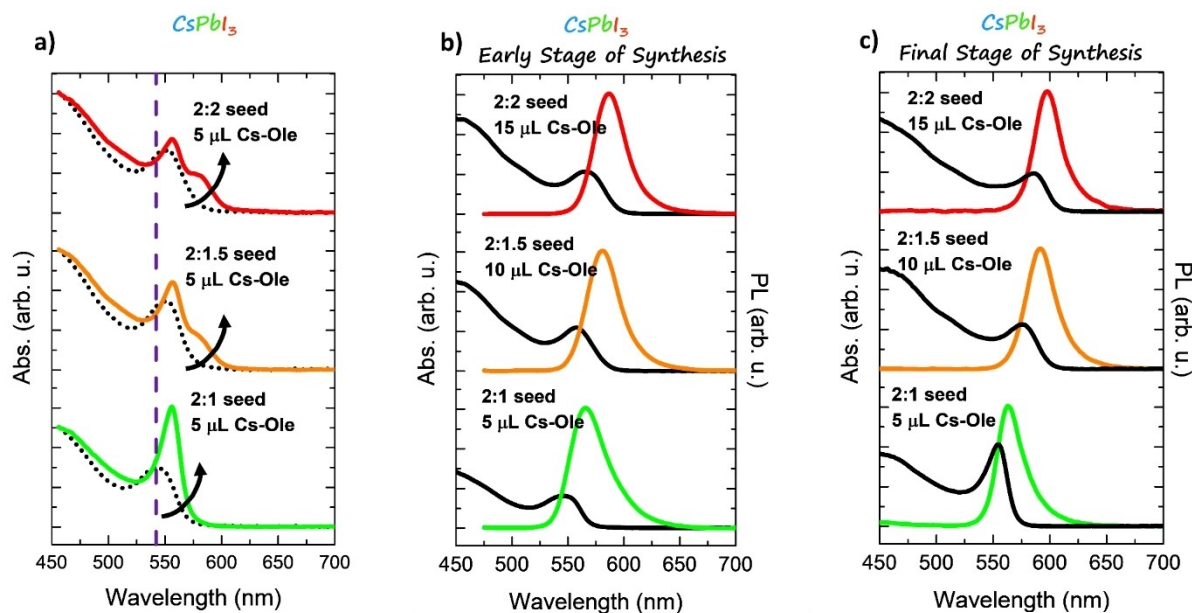


Figure 3. Seed mediated growth of NPLs. (a) The Cs-oleate volume is fixed to be 5 μL while the nanocrystal seeds have varying ligand molar ratios of OLAM/OA $2x$ ($x = 1-2$). Dashed lines and continuous lines indicate initial and final stages of the synthesis, respectively. (b, c) By decreasing OLAM/OA molar ratio used in nanocrystal seeds from 2:1 to 2:2, the amount of Cs-oleate required for the synthesis of NPLs increases. The thickness of the nanoplatelets tends to increase with a decrease in OLAM/OA ligand molar ratio.

reveal that absorption peaks of intermediate nanocrystals further shift to longer wavelengths for all samples. It should be noted that higher oleylammonium amount (by increasing oleic acid) in the reaction should be supported by higher Cs-oleate amounts for obtaining $n = 3$ NPLs as demonstrated in Figure 3c. These findings are also very similar to the bromide counterpart of LHP in the seed mediated synthesis. However, obtaining $\text{L}_2[\text{APbBr}_3]_2\text{PbBr}_4$ ($n = 2$) NPLs is much easier by using 610 mM Oca rather than 250 mM OLAM as a ligand. In fact, the synthesized $\text{L}_2[\text{APbBr}_3]_2\text{PbBr}_4$ by using OLAM transforms to $\text{L}_2[\text{APbBr}_3]_2\text{PbBr}_4$ NPLs faster than the ones synthesized by using Oca. It is known that alkylammonium cations support 2D structure and confine crystal growth by electrostatically binding to faces of crystals along one dimension.^[31] In addition, Almeida et al. have extensively investigated the acid-base equilibrium in the synthesis of cesium lead bromide nanocrystals by using hot-injection method for achieving a better understanding and control of the size, shape, and phases of nanocrystals.^[47] They have found out that alkylammonium concentration in the reaction could be increased by decreasing the reaction temperature, which may explain the low oleic acid amount ([OA] = 150 mM) required in the seed mediated method.^[47] In order to synthesize $\text{L}_2[\text{APbX}_3]_2\text{PbX}_4$ NPLs, low A-site cation concentration is required.^[31,47] In addition, $\text{L}_2[\text{CsPbI}_3]_{n-1}\text{PbI}_4$ ($n = 2, 3$) NPLs were successfully synthesized as shown in Figure S4a where Cs-oleate amount was increased from 5 μL to 20 μL for a constant OLAM/OA molar ratio of 2:1. However, we were not able to synthesize $\text{L}_2[\text{CsPbI}_3]_2\text{PbI}_4$ NPLs by using 2:1.5 and 2:2 ligand molar ratios, which may indicate that excess amount of OA inhibits binding efficiency of some alkylammonium cations and hence the synthesis yields thicker NPLs. Furthermore, it is clear that

$\text{L}_2[\text{APbBr}_3]_2\text{PbBr}_4$ NPLs could not be synthesized by using 5 μL of Cs-oleate (Figure S4b). In Figure S4b, a small shoulder observed at around 400 nm originates most likely from L_2PbBr_4 because PbBr_2 seed solution contains some amount of L_2PbBr_4 (see also Figure S5). The broad absorbance spectrum covering the wavelength range from 380 to 520 nm also confirms the incomplete formation of CsPbBr_3 NPLs. Besides, we have successfully achieved synthesis of $\text{L}_2[\text{APbBr}_3]_2\text{PbBr}_4$ NPLs by using 20 μL of Cs-oleate as shown in Figure S4b. In particular, all of the inorganic $\text{L}_2[\text{CsPbX}_3]_{n-1}\text{PbX}_4$ NPLs have very high stability. The higher stability of NPLs might be due to the combined use of oleylamine and oleic acid. In fact, the combination of oleylamine and oleic acid forms oleylammonium oleate, which bounds relatively tightly to NPL surface in a similar to the oleylammonium halides.^[48] Therefore, our method yields more stable NPLs than the previously synthesized NPLs by using the LARP (see Figure S9). In the LARP method, the synthesized Cs-based NPLs evolve thicker NPLs in several minutes to hours.^[18]

The absorption and PL spectra of the synthesized NPLs were all shown in Figure 4. In addition, the photographs in the inset show emission of colloidal LHP NPLs under UV light illumination. Note that for all A-site cations used in this work, the synthesis of APbBr_3 NPLs have slower reaction rates than APbI_3 NPLs. Furthermore, organo-lead halide perovskite NPLs were synthesized much faster than all inorganic counterparts for both APbBr_3 and APbI_3 NPLs. The faster synthesis may indicate higher diffusion kinetics of organic cations (MA^+ , FA^+) than inorganic cation (Cs^+). In addition, the growth of Cs-based LHP NPL can be accelerated by heating. Similarly, in a previous study, slow reaction kinetics in CsPbBr_3 NPLs were observed by Mehetor et al.^[35] The narrowest emission linewidth was ob-

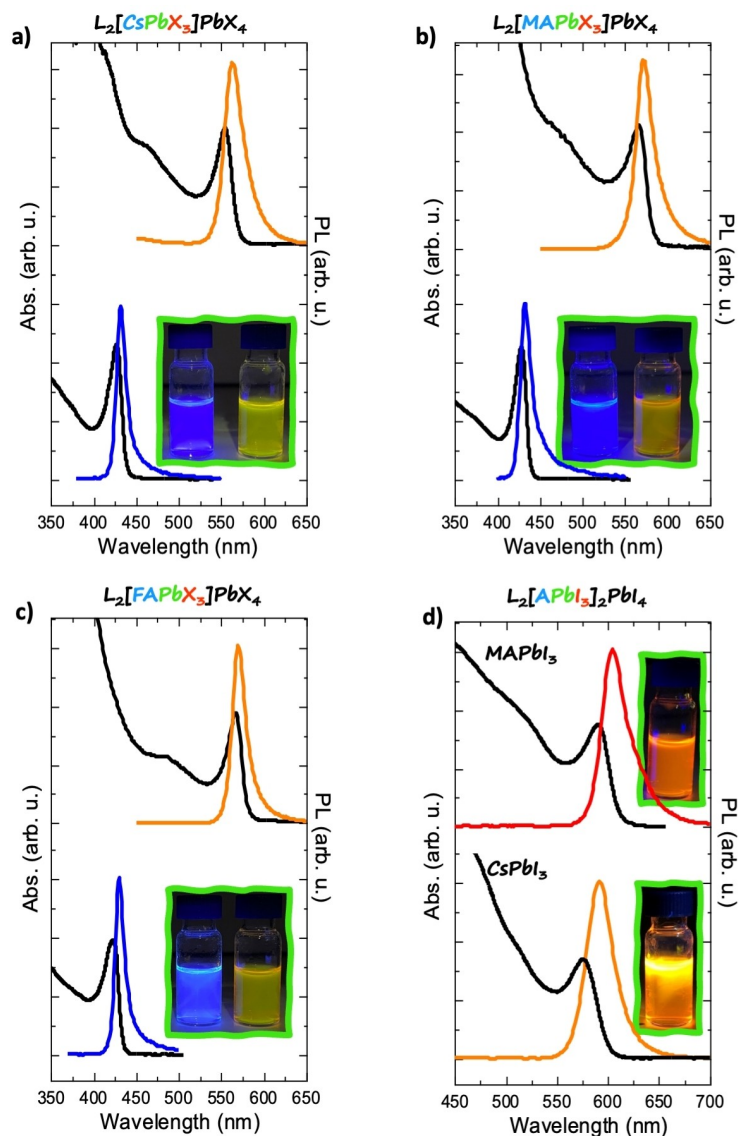


Figure 4. Absorption and PL spectra of (a) $L_2[\text{CsPbX}_3]\text{PbX}_4$, (b) $L_2[\text{MAPbX}_3]\text{PbX}_4$, (c) $L_2[\text{FAPbX}_3]\text{PbX}_4$, and (d) $L_2[\text{CsPbI}_3]_2\text{PbI}_4$ and $L_2[\text{MAPbI}_3]_2\text{PbI}_4$ NPLs. The insets in the graphs display images of the corresponding emitting NPLs under UV light illumination.

served in $L_2[\text{FAPbX}_3]\text{PbX}_4$ NPLs as shown in Figure 4c. Further, $L_2[\text{APbX}_3]\text{PbX}_4$ ($n=2$) NPLs can be synthesized using all A-site cations (FA, MA, and Cs) as demonstrated in Figure 4a and c. Also, MA and Cs cations support $L_2[\text{APbX}_3]_2\text{PbX}_4$ ($n=3$) NPLs, see Figure 4d, and Figure S6 for the absorption and PL spectra, respectively. However, we were not able to synthesize homogeneous $L_2[\text{FAPbX}_3]_2\text{PbX}_4$ ($n=3$) NPLs. Thus, increasing FA-oleate amount in the synthesis of NPLs yields heterogeneous thickness as shown in Figure S7. Additionally, our facile method allows large-scale synthesis of perovskite NPLs as demonstrated in Figure S8. We also examined the stability of perovskite NPLs under ambient conditions; see Figure S9 where a very slight redshift after certain time was observed in the absorption and PL spectra. Notably, LHPs have weak structural bonds and their bonds with the ligand shells are very weak and highly dynamic, which makes them very sensitive to polar solvents. In fact,

performing synthesis of LHP NPLs in the presence of polar solvents can decrease stability of the NPLs due to their weakly bonded nature.^[19,49] The deterioration of thickness uniformity,^[18] dissociation to precursor salts,^[50–52] and transformation to wide and indirect band gap phases^[53–54] are main problems for 2D LHP NPLs and 3D LHPs. These problems can be primarily triggered and promoted by the presence of residual polar solvents in the colloid. Therefore, the main reason for increased stability of our synthesized NPLs could be polar solvent free synthesis.

We have tuned optical properties of the NPLs by using the fast and facile anion exchange reaction approach as shown in Figure 5. In previous studies, postsynthetic anion exchange reactions were commonly employed by using chemicals such as octadecylammonium halides, oleylammonium halides, tetrabutylammonium halides, PbX_2 powder, and methylmagnesium

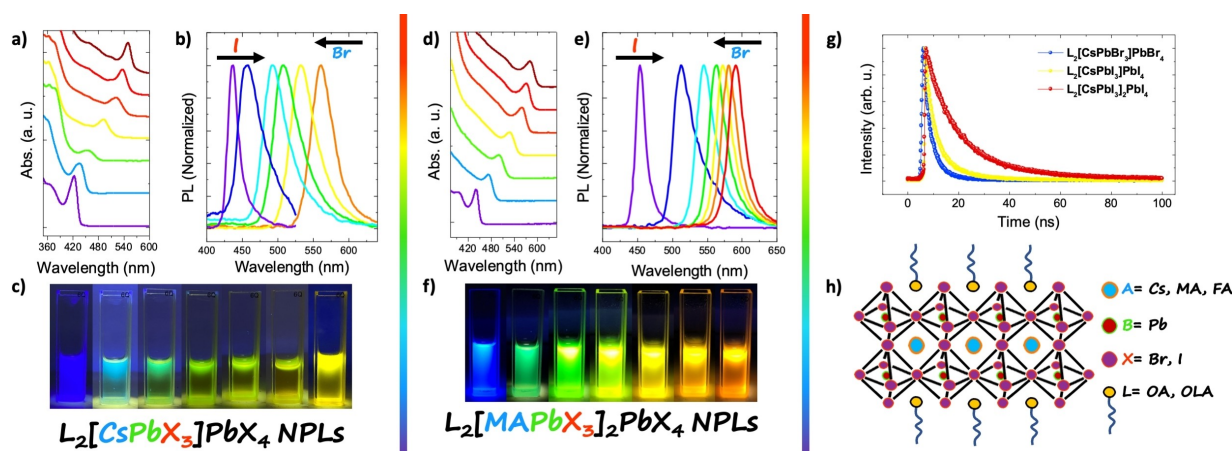


Figure 5. Tuning optical properties of colloidal metal halide perovskite nanoplatelets by varying halide content in the nanoplatelets. Halide exchange reactions of (a, b, c) $L_2[\text{CsPbX}_3]\text{PbX}_4$ NPLs, and (d, e, f) $L_2[\text{MAPbX}_3]_2\text{PbX}_4$ NPLs. (c) and (f) show emission of $L_2[\text{CsPbX}_3]\text{PbX}_4$ and $L_2[\text{MAPbX}_3]_2\text{PbX}_4$ NPLs when irradiated with a UV lamp during the halide exchange reactions, respectively. (g) Photoluminescence lifetime decay curves of $L_2[\text{CsPbBr}_3]\text{PbBr}_4$, $L_2[\text{CsPbI}_3]\text{PbI}_4$, and $L_2[\text{CsPbI}_3]_2\text{PbI}_4$ NPLs. (h) Schematic representation of $L_2[\text{APbX}_3]\text{PbX}_4$ NPLs. Each layer consists of PbX_6 octahedrons. A-site cations indeed allow formation of perovskite unit cells.

halide salts.^[55–56] Different from the previous studies, here in this study, the synthesized nanocrystal seeds enable anion exchange reaction without preparation of any additional halide precursors. It should be noted that, by mixing the desired ratios of PbI_2 and PbBr_2 nanocrystal seed colloids in the seed-mediated synthesis, mixed halide NPLs were successfully synthesized. $L_2[\text{CsPbX}_3]\text{PbX}_4$ and $L_2[\text{MAPbX}_3]_2\text{PbX}_4$ NPLs were used for anion exchange reactions, see Figure 5a and f. The mixed halide NPLs were prepared by adding 5 μL of halide nanocrystal seeds to 2 mL of NPL. After the halide exchange reaction was completed in 2 min, absorption and PL spectra of the colloid were acquired. On the other hand, photoluminescence decay measurements, very useful tool for investigating dynamics of excitons in NPLs, were performed for $L_2[\text{CsPbBr}_3]\text{PbBr}_4$, $L_2[\text{CsPbI}_3]\text{PbI}_4$, and $L_2[\text{CsPbI}_3]_2\text{PbI}_4$ NPLs as shown in Figure 5g. The PL lifetime of NPLs decreases with an increase in the band gap of NPLs. Note that the band gap of the NPLs can be engineered by controlling the thickness of the NPLs (quantum confinement effect) or by altering the halide composition of NPLs. For example, CsPbBr_3 NPLs have a larger band gap than CsPbI_3 NPLs for the same thickness value.^[30] The calculated average PL lifetimes from biexponential function fits

are 18.81 ns, 9.17 ns, and 5.05 ns for $L_2[\text{CsPbI}_3]_2\text{PbI}_4$, $L_2[\text{CsPbI}_3]\text{PbI}_4$, and $L_2[\text{CsPbBr}_3]\text{PbBr}_4$ NPLs, respectively, see Table S1 for non-radiative and radiative recombination times and their corresponding percentages.

Absorption and emission spectra of the synthesized NPLs have very similar peak positions to the previously reported absorption and emission peaks (see Table 1).^[18] However, a few differences have been observed. Firstly, almost all of the synthesized NPLs excluding $[\text{FAPbI}_3]\text{PbI}_4$ have slightly larger emission linewidths than the previously synthesized NPLs using the LARP.^[18] Secondly, the PLQY values obtained in this work are relatively higher than the previously obtained PLQY in $L_2[\text{APbX}_3]\text{PbX}_4$ NPLs.^[4,18,20,32] Thirdly, in $L_2[\text{APbBr}_3]\text{PbBr}_4$ NPLs, cation size induced red shift was not observed. It should be noted here that large cations in A-site generates narrow bandgap in the perovskite nanoplatelets.^[18] Lastly, the $[\text{FAPbBr}_3]\text{PbBr}_4$ NPLs have the largest band gap in the $[\text{APbBr}_3]\text{PbBr}_4$ NPLs and, the $[\text{FAPbBr}_3]\text{PbBr}_4$ NPLs have 37.6% PLQY, which is the highest PLQY observed in the $L_2[\text{APbX}_3]\text{PbX}_4$ NPLs synthesized in this work. Importantly, among the $L_2[\text{APbI}_3]\text{PbI}_4$ NPLs, synthesized in this study, $L_2[\text{CsPbI}_3]\text{PbI}_4$ have the highest PLQY, 12.4%. On the other hand, $L_2[\text{CsPbI}_3]_2\text{PbI}_4$ and $L_2[\text{MAPbI}_3]_2\text{PbI}_4$

Table 1. Comparison of the optical properties of the synthesized NPLs.

| | Thickness [n] | Absorption | | Emission | | FWHM [meV] | QY [%] |
|---------------------------------------|---------------|------------|------|----------|------|------------|--------|
| | | nm | eV | nm | eV | | |
| $L_2[\text{CsPbBr}_3]\text{PbBr}_4$ | 2 | 427 | 2.90 | 432 | 2.87 | 85 | 23.6 |
| $L_2[\text{CsPbBr}_3]_2\text{PbBr}_4$ | 3 | 441 | 2.81 | 449 | 2.76 | 123 | 42.7 |
| $L_2[\text{MAPbBr}_3]\text{PbBr}_4$ | 2 | 428 | 2.89 | 432 | 2.87 | 90 | 32.6 |
| $L_2[\text{MAPbBr}_3]_2\text{PbBr}_4$ | 3 | 445 | 2.78 | 451 | 2.75 | 97 | 60.8 |
| $L_2[\text{FAPbBr}_3]\text{PbBr}_4$ | 2 | 422 | 2.93 | 430 | 2.88 | 90 | 37.6 |
| $L_2[\text{CsPbI}_3]\text{PbI}_4$ | 2 | 556 | 2.23 | 563 | 2.20 | 104 | 12.4 |
| $L_2[\text{CsPbI}_3]_2\text{PbI}_4$ | 3 | 577 | 2.14 | 592 | 2.09 | 106 | 33.8 |
| $L_2[\text{MAPbI}_3]\text{PbI}_4$ | 2 | 566 | 2.19 | 572 | 2.17 | 90 | 4.14 |
| $L_2[\text{MAPbI}_3]_2\text{PbI}_4$ | 3 | 584 | 2.12 | 604 | 2.05 | 99 | 13.9 |
| $L_2[\text{FAPbI}_3]\text{PbI}_4$ | 2 | 566 | 2.19 | 570 | 2.18 | 68 | 1.66 |

NPLs have 33.8% and 13.9% PLQYs. $L_2[\text{CsPbBr}_3]_2\text{PbBr}_4$ and $L_2[\text{MAPbBr}_3]_2\text{PbBr}_4$ NPLs have 42.7% and 60.8% PLQYs, respectively. The highest PLQY obtained in this study is 60.8%, which has been observed in $L_2[\text{MAPbBr}_3]_2\text{PbBr}_4$ NPLs.

3. Conclusions

In summary, for the first time, we report seed-mediated synthesis of $L_2[\text{APbX}_3]_2\text{PbX}_4$ ($n=2$), and $L_2[\text{APbX}_3]_2\text{PbX}_4$ ($n=3$) NPLs without using A-site cation halide salt (AX; A=Cesium, methylammonium, formamidinium and, X=Cl, Br, I) and long chain alkylammonium halide salts (LX; L=oleylammonium, octylammonium, butylammonium and, X=Cl, Br, I). The synthesis of NPLs was performed in hexane by reacting nanocrystal seeds with A-site cation precursors at ambient conditions. The high resolution transmission electron microscopy measurements reveal that the synthesized nanocrystal seeds are in a circular shape and have a diameter of around 3 nm. In addition, the growth of $L_2[\text{CsPbX}_3]_2\text{PbX}_4$ NPLs was studied by optical absorption measurements where (i) sharpened excitonic absorption peaks, (ii) decrease in the linewidth of both absorption and emission peaks, and (iii) red-shift in the excitonic absorption peaks were all observed at the same time. In addition, the ligand molar ratio (OLAM/OA) in the synthesis of nanocrystal seeds is a very crucial factor controlling the thickness and homogeneity of NPLs. For example, $L_2[\text{APbI}_3]_2\text{PbI}_4$ NPLs can only be synthesized by using nanocrystal seeds with an OLAM/OA molar ratio of 2. Importantly, our facile synthesis method provides highly stable, monodisperse $L_2[\text{APbX}_3]_{n-1}\text{PbX}_4$ NPLs with very narrow absorption and emission linewidths, and high PLQYs. Moreover, by mixing the synthesized LHP NPLs with the counter halide nanocrystal seeds, the optical properties of the NPLs can be affectively tuned by halide exchange reactions. We envision that the seed mediated synthesis of perovskite nanoplatelets reported here provides further understanding of the growth dynamics of LHP NPLs.

Experimental Section

Chemicals. Lead (II) iodide (PbI_2 , 99%), lead (II) bromide (PbBr_2 , $\geq 98\%$), cesium carbonate (Cs_2CO_3 , 99.9%), formamidinium acetate salt (FA-acetate, 99.9%), methylamine solution (MA solution, 33 wt% in absolute ethanol), 1-octadecene (ODE, 90%), oleylamine (OLAM, 70%), octylamine (OcA, 99%), oleic acid (OA, 90%), and hexane (EMPLURA®) were all purchased from Sigma-Aldrich and used without any further purification.

Synthesis of Cs-Oleate. 350 mg of Cs_2CO_3 , 20 mL of ODE, and 1.25 mL of OA were all loaded into a round bottom glass flask and dried under vacuum for 1 h at 120 °C. After degassing process, the reaction temperature was increased to 150 °C under the flow of nitrogen gas and then Cs-oleate was obtained after 2 h. Before its use in the synthesis of NPLs, Cs-oleate solution was heated to 100 °C in order to completely dissolve Cs-oleate in ODE.

Synthesis of FA-Oleate (method 1). 521 mg of FA-acetate, 16 mL of ODE, and 4 mL of OA were mixed in a round bottom flask. Afterwards, the mixture was degassed at room temperature for 10 min and, additionally, degassed at 80 °C for 10 min. The temperature of the reaction vessel was set to 135 °C under the nitrogen atmosphere and kept in the same temperature until a clear solution was obtained. The FA-oleate solution was heated to 100 °C from 25 °C in order to completely dissolve FA-oleate in ODE.

Synthesis of FA-Oleate (method 2). 52 mg of FA-acetate was dissolved in 2.5 mL of OA under ultrasonication until a clear solution was obtained. The final solution was stored under ambient condition for further use.

Preparation of MA-Solution. 0.5 mL and 1 mL methylamine solutions (MA solution, 33 wt% in absolute ethanol) were diluted with 9.5 mL and 9 mL hexane for the synthesis of $L_2[\text{MAPbX}_3]_2\text{PbX}_4$ and $L_2[\text{MAPbX}_3]_2\text{PbX}_4$ NPLs, respectively.

Synthesis of nanocrystal seeds. 2 mL of ODE, 0.2 mmol PbX_2 (PbBr_2 or PbI_2) salt, 200 μL of OLAM or 250 μL of OcA, and 100–200 μL of OA were loaded into a glass tube and degassed at 80 °C and, subsequently, heated to 140–150 °C until the solution became completely clear. Then, the reaction solution was immediately quenched in an ice-water bath.

CsPbX₃ nanoplatelet synthesis. $L_2[\text{CsPbX}_3]_{n-1}\text{PbX}_4$ NPLs having $n=2, 3$ were synthesized by mixing PbX_2 nanocrystal seed solution with Cs-oleate and then, adding the mixture into hexane. Before adding

Table 2. Synthesis parameters of colloidal 2D halide perovskite nanoplatelets.

| | Thickness [n] | A-site precursor [μL] | Seed type | Seed [μL] | Added precursor [μL] | Hexane [mL] | Temperature [°C] | Time [h] |
|---|---------------|------------------------------------|-----------|------------------------|-----------------------------------|-------------|------------------|----------|
| $L_2[\text{CsPbBr}_3]_2\text{PbBr}_4$ | 2 | 20 | OLAM | 100 | 60 | 5 | RT | ON |
| $L_2[\text{CsPbBr}_3]_2\text{PbBr}_4$ | 2 | 7 | OcA | 50 | 57 | 7.5 | 65 | 2 |
| $L_2[\text{CsPbBr}_3]_2\text{PbBr}_4$ | 3 | 15 | OcA | 50 | 65 | 7.5 | 65 | 2 |
| $L_2[\text{MAPbBr}_3]_2\text{PbBr}_4$ | 2 | 70 | OcA | 100 | 25 | 5 | RT | - |
| $L_2[\text{MAPbBr}_3]_2\text{PbBr}_4$ | 3 | 30 | OLAM | 100 | 60 | 5 | RT | ON |
| $L_2[\text{FAPbBr}_3]_2\text{PbBr}_4$ (method 1) | 2 | 30 | OLAM | 100 | 60 | 5 | RT | 4 |
| $L_2[\text{FAPbBr}_3]_2\text{PbBr}_4$ (method 2) | 2 | 15 | OLAM | 100 | 115 | 5 | RT | 4 |
| $L_2[\text{CsPbI}_3]_2\text{PbI}_4$ | 2 | 2.5 | OLAM | 50 | 52.5 | 7.5 | 45 | 1.5 |
| $L_2[\text{CsPbI}_3]_2\text{PbI}_4$ | 3 | 7 | OLAM | 50 | 57 | 7.5 | 45 | 1.5 |
| $L_2[\text{CsPbI}_3]_2\text{PbI}_4$ | 2 | 5 | OLAM | 100 | 60 | 5 | RT | 6 |
| $L_2[\text{CsPbI}_3]_2\text{PbI}_4$ | 3 | 20 | OLAM | 100 | 60 | 5 | RT | 6 |
| $L_2[\text{MAPbI}_3]_2\text{PbI}_4$ | 2 | 7.5 | OLAM | 100 | 60 | 5 | RT | - |
| $L_2[\text{MAPbI}_3]_2\text{PbI}_4$ | 3 | 30 | OLAM | 100 | 60 | 5 | RT | - |
| $L_2[\text{FAPbI}_3]_2\text{PbI}_4$ | 2 | 6 | OLAM | 100 | 60 | 5 | RT | - |

RT = room temperature, ON = overnight.

Cs-oleate to PbX_2 nanocrystal seed solution, Cs-oleate was cooled down to room temperature. When Cs-oleate solution became turbid white, it was added to the nanocrystal seed colloid. Note that this process is very crucial in order to prevent any early formation of large CsPbX_3 nanocrystals! Briefly, 100 μL of PbI_2 nanocrystal seed solution was mixed with 5 μL of Cs-oleate and then 60 μL of this solution was injected into 5 mL of hexane. The solution was stored under ambient conditions for 6 hours for the synthesis of $\text{L}_2[\text{CsPbI}_3]_2\text{PbI}_4$ ($n=2$) NPLs. The same procedure was applied for the synthesis of $\text{L}_2[\text{CsPbI}_3]_2\text{PbI}_4$ ($n=3$) NPLs except 20 μL of Cs-oleate was used rather than 5 μL of Cs-oleate. For the synthesis of $\text{L}_2[\text{CsPbI}_3]_2\text{PbI}_4$ NPLs, firstly, 50 μL of nanocrystal seed colloid and then 2.5 μL of Cs-oleate were all injected into the 7.5 mL of hexane, followed by stirring at room temperature for 1 min. The prepared solution was then placed in an oil bath at 45 °C and magnetically stirred for 1.5 h. $\text{L}_2[\text{CsPbI}_3]_2\text{PbI}_4$ NPLs were synthesized by using 7 μL of Cs-oleate at the same reaction temperature and reaction time. $\text{L}_2[\text{CsPbBr}_3]_2\text{PbBr}_4$ NPLs were synthesized by mixing 100 μL of PbBr_2 nanocrystal seed solution with 20 μL of Cs-oleate and then 60 μL of this solution was quickly injected into 5 mL of hexane, and finally the synthesized NPLs were stored overnight under ambient conditions before use. For faster synthesis of $\text{L}_2[\text{CsPbBr}_3]_2\text{PbBr}_4$ NPLs, 50 μL of OcA (0.2 mmol PbBr_2 , 250 μL of OcA, and 200 μL of OA in 2 mL ODE) passivated nanocrystal seed colloid and 7 μL of Cs-oleate were injected in 7.5 mL of hexane, followed by stirring at room temperature for 1 min. The prepared solution was then placed in an oil bath at 65 °C and magnetically stirred for 2 h. In order to synthesize $\text{L}_2[\text{CsPbBr}_3]_2\text{PbBr}_4$ NPLs, we used 15 μL of Cs-oleate and performed the reaction at the same reaction temperature and time. The same synthesis procedure was applied for all A-site cations used in this work. Synthesis parameters for all of the synthesized $\text{L}_2[\text{APbX}_3]_{n-1}\text{PbX}_4$ NPLs were given in Table 2. For further information about the synthesis of NPLs see also Supporting Information.

Characterization of Nanoplatelets. Scanning transmission electron microscopy (STEM) and transmission electron microscopy (TEM) analysis of NPLs were carried out in order to observe morphology of the nanocrystals (SEM; Tescan, GAIA 3, CZE, and TEM, JEOL-2100F, Japan). The samples were prepared by drop-casting diluted nanocrystal suspensions onto 200 mesh carbon-coated copper grids. Absorption (Abs), Photoluminescence (PL), and time-resolved lifetime (LT) measurements were carried out by using a FS5 Spectrofluorometer (Edinburgh Instruments, UK). For PLQY, a Xenon lamp was employed with an excitation wavelength of 350 nm. PLQY of each sample was obtained by utilizing an integrating sphere. Samples were diluted in hexane and optical properties of the nanocrystals were measured in a cylindrical quartz cuvette. In LT measurements, the samples were excited with a 350 nm laser with a pulse width of 100 ps and a repetition rate of 1 MHz. In situ absorption measurements of colloids were performed by using a balanced deuterium – tungsten halogen light source (DH2000-BAL, Ocean Optics), and a fiber coupled spectrometer (USB4000, Ocean Optics). All of the characterization measurements were performed at room temperature.

Acknowledgements

This research was supported by TUBITAK (118F523).

Conflict of Interest

The authors declare no conflict of interest.

Keywords: 2D perovskites · colloid · nanoplatelet · quantum confinement effect · seed mediated synthesis.

- [1] M. C. Weidman, A. J. Goodman, W. A. Tisdale, *Chem. Mater.* **2017**, *29*, 5019–5030.
- [2] J.-C. Blancon, J. Even, C. C. Stoumpos, M. G. Kanatzidis, A. D. Mohite, *Nat. Nanotechnol.* **2020**, *15*, 969–985.
- [3] L. C. Schmidt, A. Pertegás, S. González-Carrero, O. Malinkiewicz, S. Agouram, G. Minguez Espallargas, H. J. Bolink, R. E. Galian, J. Pérez-Prieto, *J. Am. Chem. Soc.* **2014**, *136*, 850–853.
- [4] J. A. Sichert, Y. Tong, N. Mutz, M. Vollmer, S. Fischer, K. Z. Milowska, R. García Cortadella, B. Nickel, C. Cardenas-Daw, J. K. Stolarczyk, A. S. Urban, J. Feldmann, *Nano Lett.* **2015**, *15*, 6521–6527.
- [5] C. H. Kang, I. Dursun, G. Liu, L. Sinatra, X. Sun, M. Kong, J. Pan, P. Maity, E.-N. Ooi, T. K. Ng, *Light-Sci. Appl.* **2019**, *8*, 1–12.
- [6] C. M. Guvenc, N. Polat, S. Balci, *J. Mater. Chem. C* **2020**, *8*, 16520–16526.
- [7] X. Zheng, Y. Hou, H.-T. Sun, O. F. Mohammed, E. H. Sargent, O. M. Bakr, *J. Phys. Chem. Lett.* **2019**, *10*, 2629–2640.
- [8] G. C. Papavassiliou, *Prog. Solid State Chem.* **1997**, *25*, 125–270.
- [9] M. E. Kamminga, H.-H. Fang, M. R. Filip, F. Giustino, J. Baas, G. R. Blake, M. A. Loi, T. T. M. Palstra, *Chem. Mater.* **2016**, *28*, 4554–4562.
- [10] T. Ishihara, J. Takahashi, T. Goto, *Phys. Rev. B* **1990**, *42*, 11099.
- [11] G. C. Papavassiliou, I. Koutselas, *Synth. Met.* **1995**, *71*, 1713–1714.
- [12] D. B. Mitzi, *J. Chem. Soc. Dalton Trans.* **2001**, 1–12.
- [13] A. Splendiani, L. Sun, Y. B. Zhang, T. S. Li, J. Kim, C. Y. Chim, G. Galli, F. Wang, *Nano Lett.* **2010**, *10*, 1271–1275.
- [14] K. F. Mak, C. Lee, J. Hone, J. Shan, T. F. Heinz, *Phys. Rev. Lett.* **2010**, *105*, 136805.
- [15] A. K. Geim, I. V. Grigorieva, *Nature* **2013**, *499*, 419–425.
- [16] Z. Cheng, J. Lin, *CrystEngComm* **2010**, *12*, 2646–2662.
- [17] X. Wu, M. T. Trinh, X.-Y. Zhu, *J. Phys. Chem. C* **2015**, *119*, 14714–14721.
- [18] M. C. Weidman, M. Seitz, S. D. Stranks, W. A. Tisdale, *ACS Nano*. **2016**, *10*, 7830–7839.
- [19] H. Huang, Y. Li, Y. Tong, E. P. Yao, M. W. Feil, A. F. Richter, M. Döblinger, A. L. Rogach, J. Feldmann, L. Polavarapu, *Angew. Chem. Int. Ed.* **2019**, *58*, 16558–16562; *Angew. Chem.* **2019**, *131*, 16710–16715.
- [20] Y. Bekenstein, B. A. Koscher, S. W. Eaton, P. Yang, A. P. Alivisatos, *J. Am. Chem. Soc.* **2015**, *137*, 16008–16011.
- [21] P. Tyagi, S. M. Arveson, W. A. Tisdale, *J. Phys. Chem. Lett.* **2015**, *6*, 1911–1916.
- [22] F. Bertolotti, G. Nedelcu, A. Vivani, A. Cervellino, N. Masciocchi, A. Guagliardi, M. V. Kovalenko, *ACS Nano*. **2019**, *13*, 14294–14307.
- [23] L. C. Schmidt, A. Pertegás, S. González-Carrero, O. Malinkiewicz, S. Agouram, G. Minguez Espallargas, H. J. Bolink, R. E. Galian, J. Pérez-Prieto, *J. Am. Chem. Soc.* **2014**, *136*, 850–853.
- [24] Z. Yuan, Y. Shu, Y. Tian, Y. Xin, B. Ma, *Chem. Commun.* **2015**, *51*, 16385–16388.
- [25] Z. Yuan, Y. Shu, Y. Xin, B. Ma, *Chem. Commun.* **2016**, *52*, 3887–3890.
- [26] W. Zhai, J. Lin, Q. Li, K. Zheng, Y. Huang, Y. Yao, X. He, L. Li, C. Yu, C. Liu, *Chem. Mater.* **2018**, *30*, 3714–3721.
- [27] W. Zhai, J. Lin, C. Li, S. Hu, Y. Huang, C. Yu, Z. Wen, Z. Liu, Y. Fang, C. Tang, *Nanoscale* **2018**, *10*, 21451–21458.
- [28] Z. Wen, W. Zhai, C. Liu, J. Lin, C. Yu, Y. Huang, J. Zhang, C. Tang, *RSC Adv.* **2019**, *9*, 24928–24934.
- [29] C. Liu, J. Lin, W. Zhai, Z. Wen, X. He, M. Yu, Y. Huang, Z. Guo, C. Yu, C. Tang, *RSC Adv.* **2019**, *9*, 39315–39322.
- [30] L. Protesescu, S. Yakunin, M. I. Bodnarchuk, F. Krieg, R. Caputo, C. H. Hendon, R. X. Yang, A. Walsh, M. V. Kovalenko, *Nano Lett.* **2015**, *15*, 3692–3696.
- [31] J. Cho, Y.-H. Choi, T. E. O’Loughlin, L. De Jesus, S. Banerjee, *Chem. Mater.* **2016**, *28*, 6909–6916.
- [32] Q. A. Akkerman, S. G. Motti, A. R. Srimath Kandada, E. Mosconi, V. D’Innocenzo, G. Bertoni, S. Marras, B. A. Kamino, L. Miranda, F. De Angelis, A. Petrozza, M. Prato, L. Manna, *J. Am. Chem. Soc.* **2016**, *138*, 1010–1016.
- [33] S. Sun, D. Yuan, Y. Xu, A. Wang, Z. Deng, *ACS Nano*. **2016**, *10*, 3648–3657.
- [34] Y. Hassan, Y. Song, R. D. Pensack, A. I. Abdelrahman, Y. Kobayashi, M. A. Winnik, G. D. Scholes, *Adv. Mater.* **2016**, *28*, 566–573.
- [35] S. K. Mehetor, H. Ghosh, N. Pradhan, *J. Phys. Chem. Lett.* **2019**, *10*, 1300–1305.
- [36] S. K. Mehetor, H. Ghosh, N. Pradhan, *ACS Energy Lett.* **2019**, *4*, 1437–1442.

- [37] T. Udayabhaskararao, M. Kazes, L. Houben, H. Lin, D. Oron, *Chem. Mater.* **2017**, *29*, 1302–1308.
- [38] O. Vybornyi, S. Yakunin, M. V. Kovalenko, *Nanoscale*. **2016**, *8*, 6278–6283.
- [39] L. Protesescu, S. Yakunin, M. I. Bodnarchuk, F. Krieg, R. Caputo, C. H. Hendon, R. X. Yang, A. Walsh, M. V. Kovalenko, *Nano Lett.* **2015**, *15*, 3692–3696.
- [40] R. Grisorio, D. Conelli, R. Giannelli, E. Fanizza, M. Striccoli, D. Altamura, C. Giannini, I. Allegretta, R. Terzano, G. P. Suranna, *Nanoscale*. **2020**, *12*, 17053–17063.
- [41] W. De Gruijter, *J. Solid State Chem.* **1973**, *6*, 151–162.
- [42] Z. Zheng, A. Liu, S. Wang, Y. Wang, Z. Li, W. M. Lau, L. Zhang, *J. Mater. Chem.* **2005**, *15*, 4555–4559.
- [43] G. Pellegrino, S. D'Angelo, I. Deretzis, G. G. Condorelli, E. Smecca, G. Malandrino, A. La Magna, A. Alberti, *J. Phys. Chem. C* **2016**, *120*, 19768–19777.
- [44] D. Parobek, Y. Dong, T. Qiao, D. H. Son, *Chem. Mater.* **2018**, *30*, 2939–2944.
- [45] P. Hang, J. Xie, G. Li, Y. Wang, D. Fang, Y. Yao, D. Xie, C. Cui, K. Yan, J. Xu, D. Yang, X. Yu, *iScience*. **2019**, *21*, 217–227.
- [46] A. B. Pun, S. Mazzotti, A. S. Mule, D. J. Norris, *Acc. Chem. Res.* **2021**, *54*, 1545–1554.
- [47] G. Almeida, L. Goldoni, Q. Akkerman, Z. Dang, A. H. Khan, S. Marras, I. Moreels, L. Manna, *ACS Nano*. **2018**, *12*, 1704–1711.
- [48] J. De Roo, M. Ibanez, P. Geiregat, G. Nedelcu, W. Walravens, J. Maes, J. C. Martins, I. Van Driessche, M. V. Kovalenko, Z. Hens, *ACS Nano*. **2016**, *10*, 2071–2081.
- [49] L. Liu, S. Huang, L. Pan, L. J. Shi, B. Zou, L. Deng, H. Zhong, *Angew. Chem. Int. Ed.* **2017**, *56*, 1780–1783; *Angew. Chem.* **2017**, *129*, 1806–1809.
- [50] M. Saliba, T. Matsui, J.-Y. Seo, K. Domanski, J.-P. Correa-Baena, M. K. Nazeeruddin, S. M. Zakeeruddin, W. Tress, A. Abate, A. Hagfeldt, *Energy Environ. Sci.* **2016**, *9*, 1989–1997.
- [51] W. Chen, Y. Wu, Y. Yue, J. Liu, W. Zhang, X. Yang, H. Chen, E. Bi, I. Ashraf, M. Grätzel, *Science* **2015**, *350*, 944–948.
- [52] M. N. An, S. Park, R. Brescia, M. Lutfullin, L. Sinatra, O. M. Bakr, L. De Trizio, L. Manna, *ACS Energy Lett.* **2021**, *6*, 900–907.
- [53] A. Dutta, N. Pradhan, *ACS Energy Lett.* **2019**, *4*, 709–719.
- [54] C. M. Guvenc, Y. Yalcinkaya, S. Ozen, H. Sahin, M. M. Demir, *J. Phys. Chem. C* **2019**, *123*, 24865–24872.
- [55] Q. A. Akkerman, V. D'Innocenzo, S. Accornero, A. Scarpellini, A. Petrozza, M. Prato, L. Manna, *J. Am. Chem. Soc.* **2015**, *137*, 10276–10281.
- [56] G. Nedelcu, L. Protesescu, S. Yakunin, M. I. Bodnarchuk, M. J. Grotevent, M. V. Kovalenko, *Nano Lett.* **2015**, *15*, 5635–5640.

Manuscript received: August 6, 2021

Revised manuscript received: September 6, 2021

Accepted manuscript online: September 7, 2021

Version of record online: September 27, 2021